High Nuclearity Complexes of Lanthanide Involving Tetrathiafulvalene Ligands: Structural, Magnetic, and PhotoPhysical Properties

Fabrice Pointillart,*,[†] Boris Le Guennic,[†] Stéphane Golhen,[†] Olivier Cador,[†] Olivier Maury,[‡] and Lahcène Ouahab[†]

[†]Organométalliques: Matériaux et Catalyse, UMR 6226 CNRS-UR1 Institut des Sciences Chimiques de Rennes, Université de Rennes 1, 35042, Rennes Cedex, France

[‡]Laboratoire de Chimie de l'ENS-Lyon-UMR 5182 CNRS—ENS Lyon, Université de Lyon 1, 46 Allée d'Italie, 69364 Lyon Cedex 07, France

S *Supporting Information*

ABSTRACT: The reaction between the tetrakis(2-pyridyl-*N*-oxidemethylthio)-tetrathiafulvalene ligand (**L**) and Ln(hfac)$_3$·2H$_2$O precursors (where hfac$^-$ = 1,1,1,5,5,5-hexafluoroacetylacetonate anion and Ln = Tb^{III} (**1**), Dy^{III} (**2**), Er^{III} (**3**), and Yb^{III} (**4**) and (**4b**)) leads to the formation of five tetranuclear complexes of formula [Ln$_4$(hfac)$_{12}$(**L**)$_2$]$_n$·xCHCl$_3$·yC$_6$H$_{14}$ (n = 1, x = 2, y = 0 for (**1**), (**2**), and (**4**), n = 1, x = 4 for (**3**), and n = 2, x = 2.5, y = 1 for (**4b**)). Their X-ray structures reveal that the surrounding of each Ln^{III} center is filled by two *N*-oxide groups coming from two different ligands **L**. These tetranuclear complexes have the highest nuclearity which is reported until now for coordination compounds of lanthanide involving TTF-based ligands. Direct current (dc) measurements highlight the paramagnetic behavior of the compounds with a significant crystal field effect. The temperature dependences of static magnetic measurements for **4** have been fitted. The ground state corresponds to M_J = ±5/2 while the first excited state (M_J = ±3/2) was localized at +214 cm^{-1} which was well correlated with the luminescence transition. UV–visible absorption properties have been experimentally measured and rationalized by time-dependent density functional theory (TD-DFT) calculations. Upon irradiation at 77 K and room temperature, in the range 24390–20835 cm^{-1}, both compounds **3** and **4** display a metal-centered luminescence attributed to $^4I_{13/2} \rightarrow ^4I_{15/2}$ (6660 cm^{-1}) and $^2F_{5/2} \rightarrow ^2F_{7/2}$ (signal centered around the value of 9966 cm^{-1}) transitions, respectively. The observed six transitions could be attributed to the M_J state splitting due to the existence of two Yb1 and Yb2 ions with slightly different polyhedra in **4**.
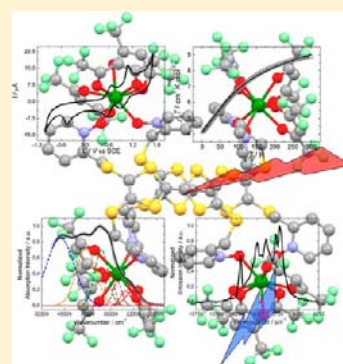
INTRODUCTION

Research and design of new multifunctional materials based on tetrathiafulvalene (TTF) is a recent challenge.[1] The idea is to combine the redox activity of such ligand with magnetic metal ions to elaborate magnetic conductors.[2] Recently, 4f lanthanide ions have been employed instead of 3d ions. The motivation for using 4f elements takes its origin in their large spins and pronounced spin–orbit coupling, in particular for Dy^{III} and Tb^{III} ions, giving a strong Ising-type magnetic anisotropy[3] suitable for building a Single Ion Magnet (SIM), Single Molecule Magnet (SMM), and Single Chain Magnet (SCM).[4] In addition, lanthanides are widely studied for their specific luminescence properties with emission lines ranging from visible to the near-infrared (NIR) spectral range and the luminescence lifetime from microsecond to millisecond range. That allows time-gated detection and large pseudo-Stokes shifts considering a ligand excitation.[5] More specifically, the NIR emitters have some potential applications in medicine because of the transparency of biological tissues to electromagnetic radiation in the range 0.8–1.3 μm.[6] Moreover some applications in optical telecommunication devices can be envisaged.[7]

The "through space" approach has been used during the past decade to obtain π-f salts.[8] To combine the electronic conductivity to the specific properties coming from the 4f elements, the "through bond" approach seems a better choice. This approach has permitted the design of coordination complexes involving both 4f ions and TTF ligands, with exciting luminescence properties[9] and SIM/SMM behavior.[10] The luminescence has been observed because of the efficient antenna effect played by the TTF ligands upon irradiation in the Intra-Ligand Charge Transfer (ILCT)[9] while molecular magnets are obtained thanks to both the Ising Dy^{III} ion and the structural role played by the TTF ligands.[10] It is worth noticing that this "through bond" approach is also suitable to combine both 3d and 4f ions with TTF ligands to reach π-3d4f systems.[11]

In a synthetic point of view, ligands offering the possibility of several coordination sites are expected to be versatile building blocks in the preparation of molecular materials. They can lead to the formation of polynuclear compounds or molecular networks.

In this way, the TTF core has been tetra-functionalized by 2-, 3-, and 4-pyridylmethylthio,[12] 2-pyrazylmethylthio,[13] cyanomethylthio,[14] 2-pyridyl- and 2-pyrazylethylthio[15] arms, but examples of coordination to metallic ions are still very scarce.[15,16] In these lines, we functionalized the TTF core with four 2-pyridyl-N-oxidemethylthio arms to elaborate complexes with the highest possible nuclearity with magnetic and luminescent properties. The reactions between the tetrakis(2-pyridyl-N-oxidemethylthio)tetrathiafulvalene ligand (**L**) (Scheme 1) and

Scheme 1. Representation of the Ligand L

(**L**)
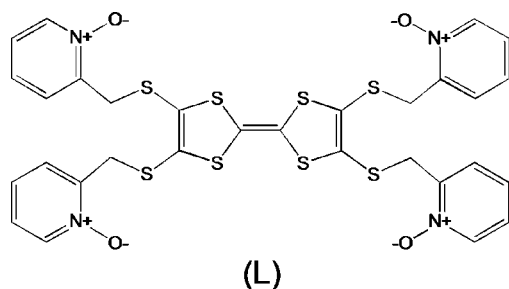
the Ln(hfac)$_3$·2H$_2$O precursors (where hfac$^-$ = 1,1,1,5,5,5-hexafluoroacetylacetonate anion and Ln = Tb^{III}, Dy^{III}, Er^{III} and Yb^{III}) lead to the formation of five tetranuclear complexes of formula [Ln$_4$(hfac)$_{12}$(**L**)$_2$]$_n$·xCHCl$_3$·yC$_6$H$_{14}$. The samples have been characterized by single crystal X-ray diffraction, magnetic measurements, UV−visible absorption, and IR emission spectroscopy. The optical properties of the ligand **L** have been rationalized by density functional theory (DFT) and time-dependent DFT (TD-DFT) calculations.

■ EXPERIMENTAL SECTION

General Procedures and Materials. All solvents were dried using standard procedures for the synthesis of **L** while standard solvents were used for the reactions of coordination. The precursors Ln(hfac)$_3$·2H$_2$O

(Ln^{III} = Tb, Dy, Er and Yb; hfac$^-$ = 1,1,1,5,5,5-hexafluoroacetylacetonate anion) were synthesized following previously reported methods.[17] All other reagents were purchased from Aldrich Co., Ltd. and used without further purification.

Crystallography. Single crystals of **1**−**4b** were mounted on a APEXII Bruker-AXS diffractometer for data collection (MoK$_\alpha$ radiation source, λ = 0.71073 Å), from the Centre de Diffractométrie (CDIFX), Université de Rennes 1, France. Structures were solved with a direct method using the SIR-97 program and refined with a full matrix least-squares method on F^2 using the SHELXL-97 program[18] for **2**−**4b** while only a cell determination was performed for **1**. Crystallographic data are summarized in Table 1. Complete crystal structure results as a CIF file including bond lengths, angles, and atomic coordinates are available as Supporting Information.

Physical Measurements. The elementary analysis of the **L** and **1**−**4b** compounds were done using SEM (Scanning Electron Microscopy). All observations and measurements were carried out with a JEOL JSM 6400 scanning electron microscope (JEOL Ltd., Tokyo, Japan) with an EDS (Energy Dispersive Spectrometry) analysis system (OXFORD Link INCA). The voltage was kept at 9 kV, and the samples were mounted on carbon stubs and coated for 5 min with a gold/palladium alloy using a sputter coater (Jeol JFC 1100). This analysis has been performed by the "Centre de Microscopie Electronique à Balayage et microAnalyse (CMEBA)" from the University of Rennes 1 (France).

^{1}H NMR was recorded on a Bruker AC 400 spectrometer. Chemical shifts are reported in parts per million referenced to TMS for ^{1}H NMR.

Cyclic voltametry was carried out in CH$_2$Cl$_2$ solution, containing 0.1 M ^{n}Bu$_4$NPF$_6$ as supporting electrolyte. Voltamograms were recorded at 100 mV s^{-1} at a platinum disk electrode. The potentials were measured versus a saturated calomel electrode (SCE).

Absorption spectra were recorded on a Varian Cary 5000 UV−visible−NIR spectrometer equipped with an integration sphere. The luminescence spectra were measured using a Horiba-Jobin Yvon Fluorolog-3 spectrofluorimeter, equipped with a three slit double grating excitation and emission monochromator with dispersions of 2.1 nm/mm (1200 grooves/mm). The steady-state luminescence was excited by unpolarized light from a 450 W xenon CW lamp and detected at an angle of 90° for diluted solution measurements or at 22.5° for solid state measurement (front face detection) by a red-sensitive Hamamatsu R928 photomultiplier tube. Spectra were reference corrected for both

Table 1. X-ray Crystallographic Data for 2−4b

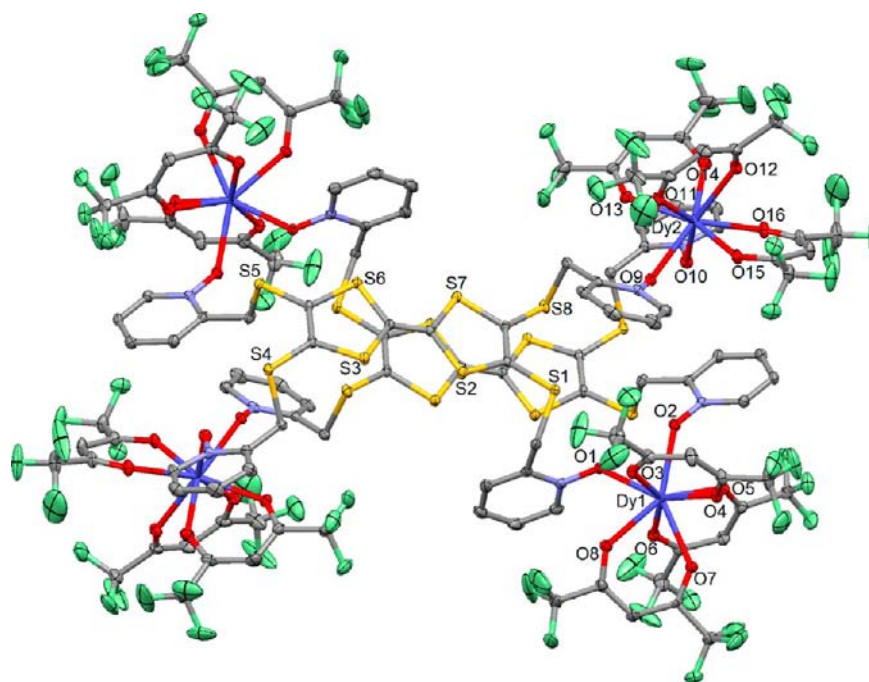| compounds	[Dy$_4$(hfac)$_{12}$(**L**)$_2$]·2CHCl$_3$ (**2**)	[Er$_4$(hfac)$_{12}$(**L**)$_2$]·4CHCl$_3$ (**3**)	[Yb$_4$(hfac)$_{12}$(**L**)$_2$]·2CHCl$_3$ (**4**)	[Yb$_4$(hfac)$_{12}$(**L**)$_2$]$_2$·2.5CHCl$_3$·C$_6$H$_{14}$ (**4b**)
formula	C$_{122}$H$_{62}$Dy$_4$F$_{72}$N$_8$O$_{32}$S$_{16}$Cl$_6$	C$_{124}$H$_{64}$Er$_4$F$_{72}$N$_8$O$_{32}$S$_{16}$Cl$_{12}$	C$_{122}$H$_{62}$Yb$_4$F$_{72}$N$_8$O$_{32}$S$_{16}$Cl$_6$	C$_{248.5}$H$_{136.5}$Yb$_8$F$_{144}$N$_{16}$O$_{64}$S$_{32}$Cl$_{7.5}$
M/g mol^{-1}	4893.0	5151.2	4935.0	9776.75
crystal system	triclinic	monoclinic	monoclinic	triclinic
space group	$P\bar{1}$ (No. 2)	$P2_1/a$ (No. 14)	$P2_1/c$ (No. 14)	$P\bar{1}$ (No. 2)
cell parameters				
a, Å	12.2911(6)	18.1845(7)	12.6633(5)	19.1532(3)
b, Å	18.8157(10)	25.8088(8)	33.5547(14)	22.5108(3)
c, Å	20.0870(10)	19.7696(8)	21.3770(10)	24.7437(3)
α, deg	75.6440(22)			94.3354(8)
β, deg	82.1162(20)	108.0258(19)	93.397(2)	97.1996(7)
γ, deg	71.7422(19)			108.9054(7)
volume/Å^3	4265.85(54)	8822.88(81)	9067.40(96)	9936.2(2)
Z	2	4	4	2
T/K	150 (2)	150 (2)	150(2)	150(2)
2θ range /deg	2.10 ≤ 2θ ≤ 54.94	2.16 ≤ 2θ ≤ 55.00	2.26 ≤ 2θ ≤ 55.32	3.56 ≤ 2θ ≤ 52.75
ρ_{calc}/g cm^{-3}	1.906	1.940	1.813	1.637
μ/mm^{-1}	2.169	2.399	2.456	2.200
no. of reflections	66613	74464	49653	54456
independent reflections	18980	20122	20745	38661
R_{int}	0.0390	0.0700	0.0597	0.0232
$F_o^2 > 2\sigma(F_o)^2$	14960	13295	12705	26895
no. of variables	1199	1235	1193	2379
R$_1$, wR$_2$	0.0400, 0.1086	0.0553, 0.1395	0.0872, 0.2008	0.0615, 0.1717

Figure 1. ORTEP view of the tetranuclear complex $[Dy_4(hfac)_{12}(L)_2] \cdot 2CHCl_3$ (**2**). Thermal ellipsoids are drawn at 30% probability. Hydrogen atoms and chloroform molecules are omitted for clarity.

the excitation source light intensity variation (lamp and grating) and the emission spectral response (detector and grating). Uncorrected NIR spectra were recorded at an angle of 45° using a liquid nitrogen cooled, solid indium/gallium/arsenic detector (850−1600 nm). The direct current (dc) magnetic susceptibility measurements were performed on solid polycrystalline sample with a Quantum Design MPMS-XL SQUID magnetometer between 2 and 300 K in applied magnetic field of 0.2 T for temperatures of 2−20 K and 1 T for temperatures of 20−300 K. These measurements were all corrected for the diamagnetic contribution as calculated with Pascal's constants.

Computational Details. DFT geometry optimizations and TD-DFT excitation energy calculations of the ligand **L** were carried out with the Gaussian 09 (revision A.02) package[19] employing the PBE0 hybrid functional.[20] All atoms were described with the SVP basis sets.[21] The first 80 monoelectronic excitations were calculated. In all steps, a modeling of bulk solvent effects (solvent = chloroform) was included through the Polarizable Continuum Model (PCM),[22] using a linear-response nonequilibrium approach for the TD-DFT step.[23] Molecular orbitals were sketched using the Gabedit graphical interface.[24]

Synthesis of Tetrakis(2-pyridyl-_N_-oxidemethylthio)-tetrathiafulvalene (L). A solution of 0.5 M EtONa/EtOH (10 mL) was added to a suspension of 2,3,6,7-tetrakis(2-cyano-ethylthio)-tetrathiafulvene[25] (0.272 g, 0.5 mmol) in anhydrous degassed EtOH (15 mL) under Argon. After being stirred at room temperature for 6 h, the mixture was reacted with a solution of 2-(chloromethyl)pyridine-1-oxide[26] (0.430 g, 3.0 mmol) in anhydrous degassed EtOH (20 mL), and then the mixture was stirred for 16 h. H_2O (20 mL) was added to quench the reaction, and the mixture was poured into CH_2Cl_2 (125 mL), washed with saturated $NaHCO_3$ (3×20 mL) and water (75 mL). The organic extract was concentrated in vacuum to give a red-brown oil which was purified by chromatography on alumina gel, initially with CH_2Cl_2 (to remove the unreacted alkyl halide) and then with CH_2Cl_2/MeOH (20:1) to give the pure desired ligand. Yield: 235 mg (62%). Anal. Calcd (%) for $C_{30}H_{24}N_4O_4S_8$: C 47.37, H 3.16, N 7.37; found: C 47.29, H 3.22, N 7.39. ^1H NMR (CDCl_3): 8.31−8.25 (m, 8H), 7.37−7.21 (m, 8H), 3.30 (s, 8H).

Synthesis of Complexes 1−4b. _[Ln_4(hfac)_{12}(L)_2]·2CHCl_3 (Ln = Tb^{III} (1) and Ln = Dy^{III} (2))._ A 0.06 mmol portion of Ln(hfac)_3·2H_2O was dissolved in 5 mL of CHCl_3 and then added to a solution of 10 mL of CHCl_3 containing 22.8 mg of **L** (0.03 mmol). After 15 min of stirring, _n_-

hexane was layered at room temperature to give orange single crystals which are suitable for X-ray studies. Yield 50 mg (68%) and 54 mg (73%) respectively for compounds **1** and **2**. Anal. Calcd (%) for $C_{120}H_{60}Tb_4F_{72}N_8O_{32}S_{16}$: C 31.04, H 1.29, N 2.41; found: C 30.85, H 1.26 N, 2.37. Anal. Calcd (%) for $C_{120}H_{60}Dy_4F_{72}N_8O_{32}S_{16}$: C 30.94, H 1.29, N 2.41; found: C 30.79, H 1.24, N 2.39.

_[Er_4(hfac)_{12}(L)_2]·4CHCl_3 (3)._ A 49.4 mg portion of Er(hfac)_3·2H_2O (0.06 mmol) was dissolved in 5 mL of CHCl_3 and then added to a solution of 10 mL of CHCl_3 containing 22.8 mg of **L** (0.03 mmol). After 15 min of stirring, _n_-hexane was layered to give orange single crystals which are suitable for X-ray study. Yield 63 mg (81%). Anal. Calcd (%) for $C_{120}H_{60}Er_4F_{72}N_8O_{32}S_{16}$: C 30.81, H 1.28, N 2.40; found: C 30.64, H 1.25, N 2.31.

_[Yb_4(hfac)_{12}(L)_2]·2CHCl_3 (4)._ A 49.7 mg portion of Yb(hfac)_3·2H_2O (0.06 mmol) was dissolved in 5 mL of CHCl_3 and then added to a solution of 10 mL of CHCl_3 containing 22.8 mg of **L** (0.03 mmol). After 15 min of stirring, _n_-hexane was layered at room temperature to give orange single crystals which are suitable for X-ray study. Yield 58 mg (79%). Anal. Calcd (%) for $C_{120}H_{60}Yb_4F_{72}N_8O_{32}S_{16}$: C 30.66, H 1.28, N 2.39; found: C 30.55, H 1.20, N 2.29.

_[Yb_4(hfac)_{12}(L)_2]_2·2.5CHCl_3·C_6H_{14} (4b)._ A 99.4 mg portion of Yb(hfac)_3·2H_2O (0.12 mmol) was dissolved in 5 mL of CHCl_3 and then added to a solution of 10 mL of CHCl_3 containing 22.8 mg of **L** (0.03 mmol). After 15 min of stirring, _n_-hexane was layered at room temperature to give orange single crystals which are suitable for X-ray study. Yield 32 mg (42%). Anal. Calcd (%) for $C_{240}H_{120}Yb_8F_{144}N_{16}O_{64}S_{32}$: C 30.66, H 1.28, N 2.39; found: C 30.65, H 1.22, N 2.35.

■ RESULTS AND DISCUSSION

Crystal-Structure Analysis of $[Ln_4(hfac)_{12}(L)_2] \cdot 2CHCl_3$ (Ln = Tb^{III} (1) and Ln = Dy^{III} (2)). Both compounds **1** and **2** are isostructural. The full data collection and the refinement of the structure have been done for **2** while the cell parameters have been determined to confirm the isomorphism of **1** (Supporting Information, Table S1). Consequently the structural description is given for **2**. It crystallizes in the $P\bar{1}$ (No. 2) triclinic space group (Table 1). The asymmetric unit is composed of two Dy(hfac)_3 moieties, two one-half ligands **L** and one chloroform molecule of

Table 2. Selected Bond Lengths for Compounds 2–4b

|	2	3	4			
					4b	
Ln1–O1	2.308(3)	2.302(4)	2.266(7)	2.273(5)	2.264(6)	Ln3–O17
Ln1–O2	2.320(3)	2.266(5)	2.304(8)	2.282(6)	2.289(6)	Ln3–O18
Ln1–O3	2.395(3)	2.327(5)	2.327(8)	2.374(5)	2.324(7)	Ln3–O19
Ln1–O4	2.364(4)	2.333(5)	2.284(8)	2.335(6)	2.305(8)	Ln3–O20
Ln1–O5	2.325(3)	2.368(5)	2.306(8)	2.283(7)	2.332(6)	Ln3–O21
Ln1–O6	2.412(3)	2.337(5)	2.292(8)	2.341(6)	2.301(8)	Ln3–O22
Ln1–O7	2.353(3)	2.357(5)	2.302(7)	2.314(6)	2.264(9)	Ln3–O23
Ln1–O8	2.340(3)	2.384(5)	2.340(9)	2.328(5)	2.316(7)	Ln3–O24
Ln2–O9	2.348(3)	2.287(5)	2.300(8)	2.292(5)	2.233(6)	Ln4–O25
Ln2–O10	2.338(3)	2.308(4)	2.251(9)	2.246(5)	2.299(5)	Ln4–O26
Ln2–O11	2.359(3)	2.327(5)	2.296(10)	2.349(6)	2.323(7)	Ln4–O27
Ln2–O12	2.367(3)	2.384(5)	2.305(8)	2.303(6)	2.300(7)	Ln4–O28
Ln2–O13	2.399(3)	2.322(4)	2.328(10)	2.268(6)	2.322(8)	Ln4–O29
Ln2–O14	2.370(3)	2.365(5)	2.322(9)	2.332(6)	2.345(7)	Ln4–O30
Ln2–O15	2.338(3)	2.359(5)	2.278(9)	2.315(6)	2.276(8)	Ln4–O31
Ln2–O16	2.382(3)	2.327(5)	2.365(10)	2.382(7)	2.335(7)	Ln4–O32
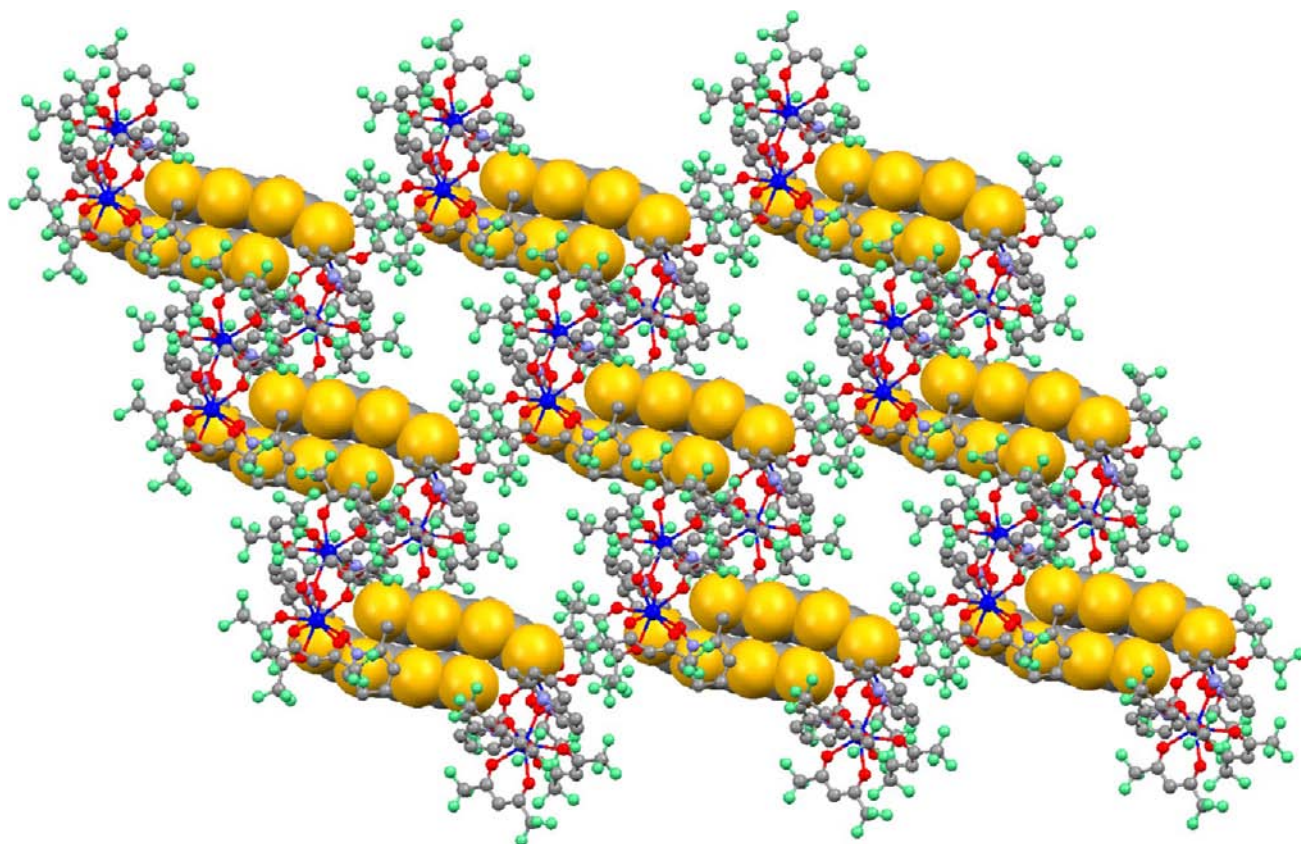
Figure 2. Crystal packing of **2** highlighting the formation of dimers of **L** (spacefill representation).

crystallization (Figure 1). The tetranuclear complexes are generated by the inversion center. Each Dy^{III} ion is surrounded by eight oxygen atoms that belong to three hfac$^-$ ligands and two crystallographically independent one-half monochelating ligands **L**. The average Dy–O_L distances are shorter (2.329(3) Å) than the average Dy–O_{hfac} distances (2.367(3) Å) (Table 2) because of the difference of Lewis base character. The arrangement of the ligands leads to strongly distorted square antiprism (D_{4d} symmetry) as coordination polyhedra for Dy1 and Dy2 lanthanide ions. The characteristic angles for Dy1 [Dy2] have been found equal to 1.9(1) [10.3(1)], 0.6(1) [2.4(2)], 57.5(1) [59.1(1)] and 58.2(1) [56.1(1)]° which may be compared to 0.0,

0.0, 52.4 and 52.4° for a regular square antiprism.[27] The formation of the tetranuclear compound is due to the coordination of two different ligands **L** to each metal centers. On the contrary, the tetrathiafulvalene which is functionalized with the 2-pyridylethylthio arm allows the coordination of two of such arms coming from the same ligand and thus leads to the formation of dinuclear compound.[15] This is driven by the fact that the 2-pyridyl-N-oxidemethylthio arms are shorter than the 2-pyridyl-N-oxidemethylthio ones. In addition to the first remark, the arrangement of the 2-pyridine-N-oxide-methyl-sulfanyl arms drives also the intramolecular and intermolecular Ln⋯Ln distances and the crystal packing. In **2**, the intramolecular

Dy···Dy distances are equal to 8.916, 14.532, and 16.685 Å. The central C=C bond of the TTF core is equal to 1.346(6) Å that attests the neutral form of the ligand **L**. The crystal packing reveals the formation of intramolecular dimers of **L** (Figure 2) due to S3···S8 contacts (3.740(6) Å) that are in the same order of magnitude than the sum of the van der Waals radii. No intermolecular S···S contacts have been observed however the shortest intermolecular Dy···Dy distance (8.626 Å) has been found shorter than the intramolecular one.

[Er₄(hfac)₁₂(L)₂]·4CHCl₃ (3). It crystallizes in the P2₁/a (No. 14) monoclinic space group (Table 1). The asymmetric unit is composed of two Er(hfac)₃ moieties, two one-half **L** ligands and two chloroform molecules of crystallization (Figure 3). A similar
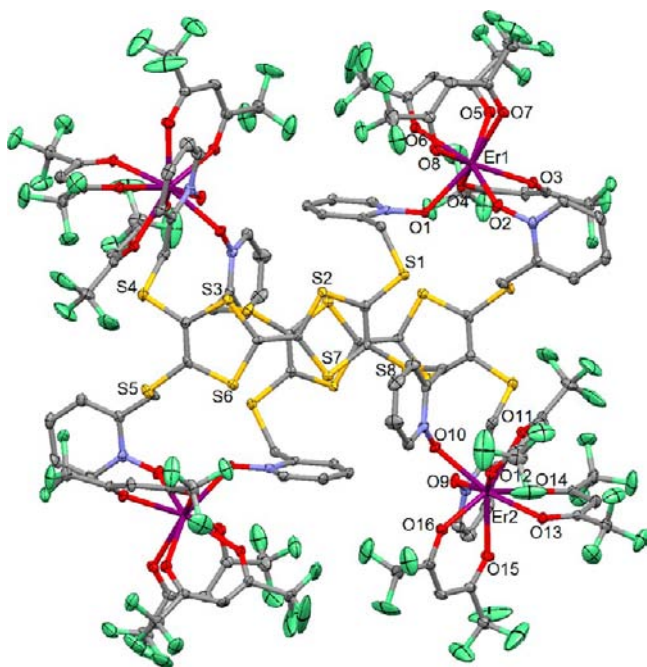

Figure 3. Ortep view of the tetranuclear complex [Er₄(hfac)₁₂(L)₂]·4CHCl₃ (**3**). Thermal ellipsoids are drawn at 30% probability. Hydrogen atoms and chloroform molecules are omitted for clarity.

tetranuclear complex than in **2** is formed, however the arrangement of the four arms leads to significant changes in the coordination polyhedra and Ln···Ln distances. Even if both Er1 and Er2 centers are coordinated to eight oxygen atoms, their surroundings can be described in two different manners. For Er1, the arrangement of the ligands leads to a slightly distorted bicapped square face trigonal prism (C_{2v} symmetry) as coordination polyhedron. The characteristic angles are equal to 4.4(2), 22.3(2), 45.6(2) and 47.5(2)° which may be compared to 0, 21.8, 48.2 and 48.2° for a regular bicapped square face trigonal prism.[27] For Er2, the coordination sphere can be described as a dodecahedron (D_{2d} symmetry) with the characteristic angles of 26.0(2), 25.1(2), 36.4(2) and 26.2(2)° compare to 29.5, 29.5, 29.5 and 29.5° for the regular polyhedron.[27] The intramolecular Er···Er distances are equal to 10.440, 11.516, and 15.490 Å. The central C=C bond of the TTF core is equal to 1.339(9) Å that attests the neutral form of the ligand **L**. The crystal packing is quite similar to the one observed for compounds **1** and **2**. It reveals the formation of intramolecular dimers of **L** (Figure 4) due to S3···S8 contacts (3.844(6) Å). No intermolecular S···S contacts have been observed however the shortest intermolec-

ular Dy···Dy distance (9.113 Å) has been found shorter than the intramolecular one.

[Yb₄(hfac)₁₂(L)₂]·2CHCl₃ (4). It crystallizes in the P2₁/c (No. 14) monoclinic space group (Table 1). The asymmetric unit is composed of two Yb(hfac)₃ moieties, two one-half ligands **L** and one chloroform molecule of crystallization (Figure 5). The arrangement of the arms of the ligand is once again different than the arrangement observed for the compounds **1−3** leading to variation in the geometry of the coordination sphere. Both crystallographically independent Yb(III) ions are localized in a strongly distorted C_{2v} symmetry (distorted bicapped square face trigonal prism) with characteristic angles of 15.8(3), 20.8(3), 54.3(3) and 53.3(3)° and 13.7(3), 17.0(3), 48.0(4) and 43.3(3)° for Yb1 and Yb2, respectively.[27] New intramolecular Yb···Yb distances equal to 9.829, 12.007, and 16.044 Å are identified. The central C=C bond of the TTF core is equal to 1.335(17) Å that attests the neutral form of the ligands **L**. The crystal packing reveals intramolecular dimers of **L** due to S2···S5 (3.774 Å) and S5···S7 (3.577 Å) contacts while the intermolecular S1···S2 contacts (3.574(6) Å) lead to the formation of one-dimensional organic network of **L** (Figure 6a). Each pseudochain of ligands **L** is structurally well isolated by the inorganic network constituted of the Yb(hfac)₃ moieties (Figure 6b). The shortest intermolecular Yb···Yb distance has been found equal to 9.925 Å.

[Yb₄(hfac)₁₂(L)₂]₂·2.5CHCl₃·C₆H₁₄ (4b). This compound was obtained using four equivalents of metallic precursor compared to the ligand. It crystallizes in the P1̄ (No. 2) triclinic space group (Table 1). The asymmetric unit is composed of two half tetranuclear molecules, 5/4 chloroform and 1/2 *n*-hexane molecules of crystallization. Each centro-symmetrical molecule is composed of four Yb(hfac)₃ moieties, coordinated to two ligands **L**, (Supporting Information, Figure S1). The TTF fragments belonging to two crystallographically independent tetranuclear molecules are almost perpendicular one to the other (Supporting Information, Figure S1). Each tetranuclear molecule can be distinguished by the coordination sphere geometry of the Yb^III ions. Yb1 and Yb2 environments have a C_{2v} symmetry (distorted bicapped square face trigonal prism) while the Yb3 and Yb4 ones have a D_{4d} symmetry (distorted square antiprism) (specific angle values are given in Supporting Information, Table S2).

The crystal packing of **4b** is totally different compared to **4**. The tetranuclear molecules are well isolated and the very large voids in the structure are filled by chloroform and *n*-hexane molecules (Supporting Information, Figure S2).

Electrochemical Properties. The redox properties of **L** and the related complexes **1−4b** are investigated by cyclic voltametry, and the oxidation potentials are listed in Table 3. The cyclic voltammogram for **L** shows two monoelectronic oxidation waves at about 0.52 and 0.95 V corresponding to the formation of a radical cation and a dication TTF fragment, respectively. These oxidation potentials are very similar to those found for the BEDT-TTF donor (0.52 and 0.94 V)[28] and the tetra-substituted TTF derivatives.[15] Upon coordination of the lanthanide, both $E^1_{1/2}$ and $E^2_{1/2}$ are anodically shifted to 0.08 and 0.04 V compared to the potentials of **L**. Complexation to the electron attracting Ln(hfac)₃ fragments enhances the electron acceptor effect of the pyridine-*N*-oxide ring leading to a decrease of the electronic density of the TTF core and so, positive shifts of $E^1_{1/2}$ and $E^2_{1/2}$ are observed (Table 3). No duplication of the oxidation waves is observed signifying that the oxidation and the reduction are simultaneous for all the donors of a complex (Supporting
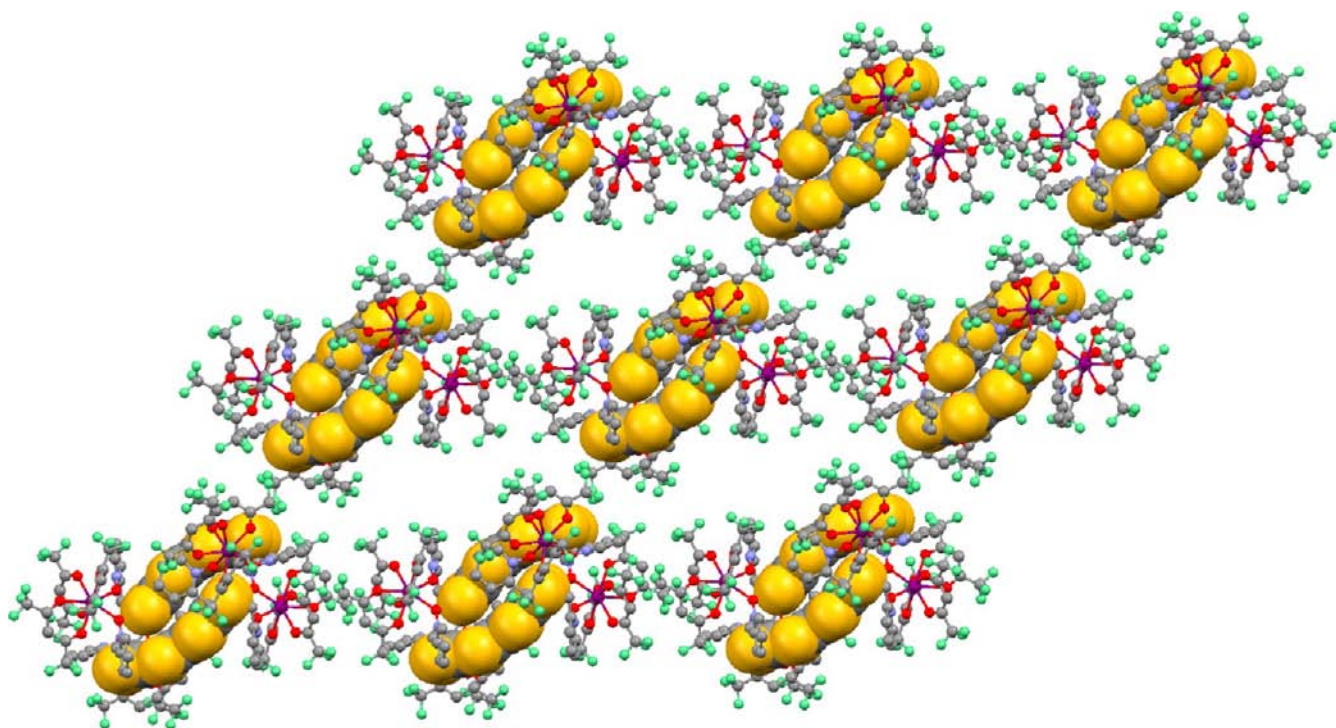
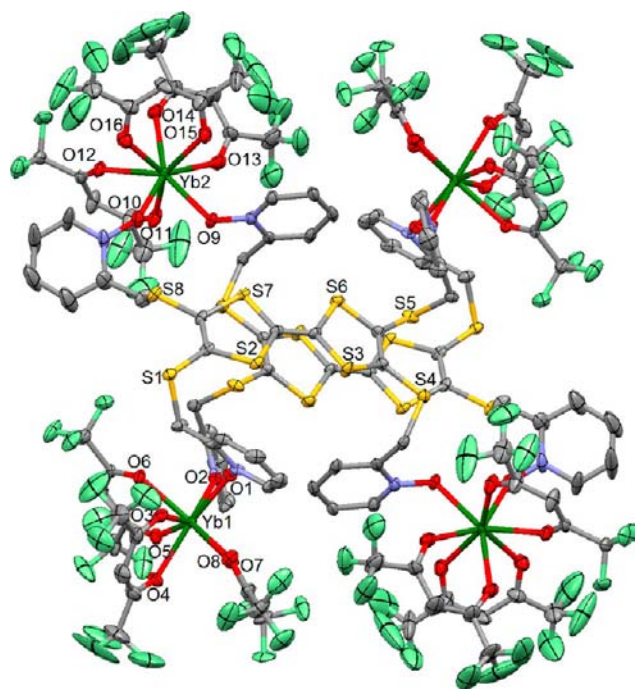**Figure 4.** Crystal packing of **3** highlighting the formation of dimers of **L** (spacefill representation).

Figure 5. Ortep view of the tetranuclear complex [Yb$_4$(hfac)$_{12}$(**L**)$_2$]·2CHCl$_3$ (**4**). Thermal ellipsoids are drawn at 30% probability. Hydrogen atoms and chloroform molecules are omitted for clarity.
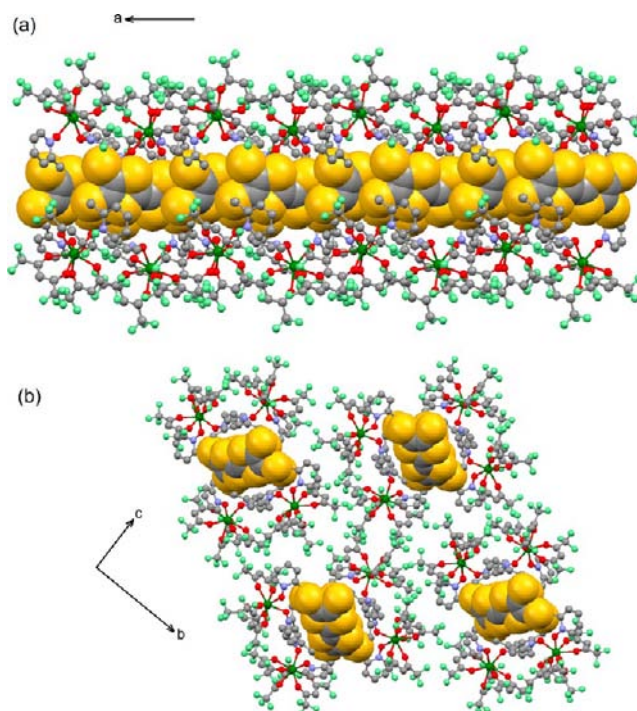

Figure 6. Crystal packing of **4** highlighting the formation of a 1D organic network of **L** along the *a* axis (spacefill representation) (a). Isolation of the 1D organic network by the inorganic one in the plane [011] (b).

Information, Figure S3). The electrochemical properties attest the redox-activity of **L** in the complexes.

Magnetic Properties. The thermal variations of the $\chi_M T$ products for **1**−**4** are given in Figure 7. All the $\chi_M T$ products show a monotonic decrease in the range of temperature 300−2 K taking the values of 47.54 and 34.41 cm^3 K mol^{-1}, 56.66 and 40.47 cm^3 K mol^{-1}, 46.03 and 21.99 cm^3 K mol^{-1}, 10.22 and 5.37

cm^3 K mol^{-1} for complexes **1**−**4**, respectively. The experimental room temperature values of $\chi_M T$ are in agreement with the theoretical value of 47.28, 56.68, 45.86, and 10.28 cm^3 K mol^{-1} expected for four magnetically isolated Tb^{III}, Dy^{III}, Er^{III}, and Yb^{III} ions.[29] The long magnetic pathway and/or metal−metal distances make impossible the existence of significant exchange and/or dipolar interaction between the paramagnetic centers.

Table 3. Oxidation Potentials[a] of the Ligand L and Complexes 1−4b

	$E^1_{1/2}$	$E^2_{1/2}$
L	0.524	0.949
1	0.599	0.995
2	0.604	0.982
3	0.597	0.979
4	0.605	0.986
4b	0.606	0.991

[a]V vs SCE, nBu$_4$NPF$_6$, 0.1 M in CH$_2$Cl$_2$ at 100 mV s^{-1}.
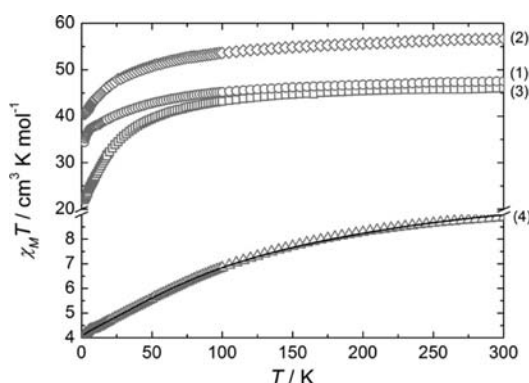

Figure 7. Thermal variation of $\chi_M T$ for **1** (circles), **2** (lozenges), **3** (squares), **4** (up-triangles), and the best fit for **4** (black line).

The first magnetization curves are depicted in Supporting Information, Figure S4 and show classical behavior in the field range 0−5 T for magnetically isolated lanthanides such as those involve in complexes **1−4**.

Photophysical Properties. *Absorption Properties.* The UV−visible absorption properties of **L** were studied in a CHCl$_3$ solution (Figure 8a) and the rationalization by TD-DFT calculations was performed (Figure 8b, Table 4). The molecular orbital diagram is depicted in Figure 9.

The calculated UV−visible absorption spectrum for **L** reproduces well the experimental curve (Figures 8a and 8b). The experimental absorption spectrum of **L** was deconvoluted into six bands. The four lowest energy bands were attributed to TTF to Methyl-2-Py-*N*-oxide charge transfers (ILCT) (red Gaussian deconvolutions). The calculated values of the absorption maxima are very close to the experimental ones. The ILCTs are identified as $\pi-\pi^*$ HOMO → LUMO (23171 cm^{-1}), HOMO → LUMO+2 (26897 cm^{-1}), HOMO → LUMO+3/+5 (average calculated value of 29189 cm^{-1}) and HOMO-1 → LUMO+8 (average calculated value of 31914 cm^{-1}). The absorption band centered at 36400 cm^{-1} (orange deconvolution) was calculated in the range of 34054−40905 cm^{-1} and attributed to Intra-Donor (TTF) (ID) transitions. Finally the highest energy absorption band centered at 43900 cm^{-1} (blue deconvolution) was attributed to Intra-Acceptor (Methyl-pyridine-N-oxide) IA transitions.

The UV−visible absorption properties of the coordination complexes **1−4** have been first studied in the solid state (Figures 10a, 11a and Supporting Information, Figure S5) and then in CHCl$_3$ solution for **4** (Figure 12a). The absorption spectra are almost identical for all complexes. Thus the absorption spectra have been deconvoluted into seven bands only for **3** and **4** since their emission properties have been also studied (Table 5). They show an additional intense absorption excitation centered at 33000 cm^{-1} compared to the free ligand (green deconvolution).
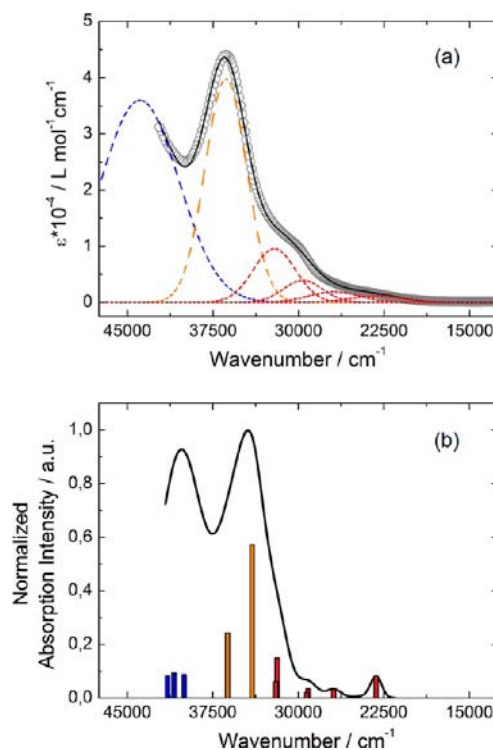
Figure 8. (a) Experimental UV−visible absorption spectra in CHCl$_3$ solution of **L** ($C = 4 \times 10^{-5}$ mol L^{-1}) (open gray circles). Respective Gaussian deconvolutions (dashed lines) and best fit (full black line) ($R = 0.99935$). (b) Theoretical absorption spectra of compounds **L** (black line). The sticks represent the mean contributions of the absorption spectra for **L**.

Table 4. TD-DFT Calculated Excitation Energies and Main Compositions of the Low-Lying Electronic Transitions for L[a]

E exp (cm^{-1})	E theo (cm^{-1})	osc.	type	assignment	transition
23100	23171	0.06	ILCT	$\pi_{TTF} \rightarrow \pi^*_{Py\text{-}N\text{-}oxide}$	H→L (80%)
26900	26897	0.02	ILCT	$\pi_{TTF} \rightarrow \pi^*_{Py\text{-}N\text{-}oxide}$	H→L+2 (81%)
29600	29128	0.03	ILCT	$\pi_{TTF} \rightarrow \pi^*_{Py\text{-}N\text{-}oxide}$	H→L+3/+5 (50/43%)
	29250	0.02			H→L+3/+5 (35/45%)
32100	31863	0.11	ILCT	$\pi_{TTF} \rightarrow \pi^*_{Py\text{-}N\text{-}oxide}$	H-1→L+8 (67%)
	31965	0.05			H-1→L+8 (30%)
36400	34054	0.42	ID	$\pi_{TTF} \rightarrow \pi^*_{TTF}$	H→L+11 (49%)
	36210	0.18			H-1→L+11/+13 (20/30%)
	40022	0.06			H-3→L+3 (25%)
	40905	0.07			H-3→L+5/+10 (7/15%)
43900			IA	$\pi_{Py\text{-}N\text{-}oxide} \rightarrow \pi^*_{Py\text{-}N\text{-}oxide}$	H-1→L+4/+8 (7/7%)
	41465	0.06			H-8→L+5 (18%)
					H-3→L+4 (8%)
					H-1→L+10 (10%)

[a]In addition, the charge transfer and the pure intramolecular transitions are reported. ID, IA and H, L represent the intramolecular TTF (Donor), intramolecular or Methyl-2-pyridine-N-oxide (acceptor), and the HOMO, the LUMO, respectively. Therefore, ILCT is for Intra-Ligand Charge Transfer. The theoretical values are evaluated at the PCM(CHCl3)-PBE0/SVP level of approximation.
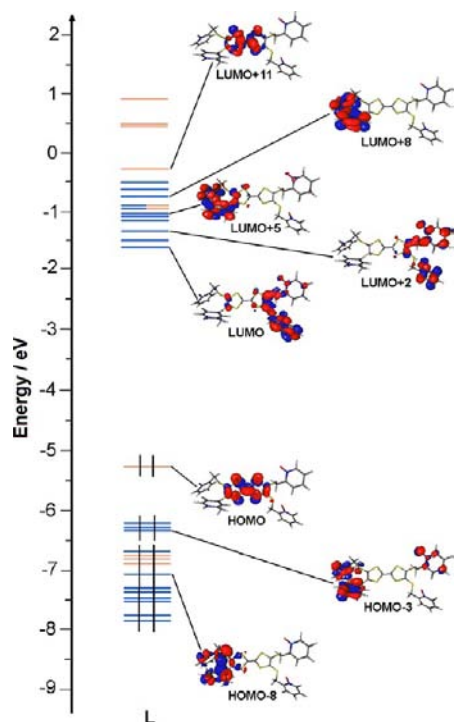
Figure 9. MO diagram of **L**. Energy levels of the centered TTF donor and methyl-2-Py-*N*-oxide acceptor are represented in orange and blue color, respectively.
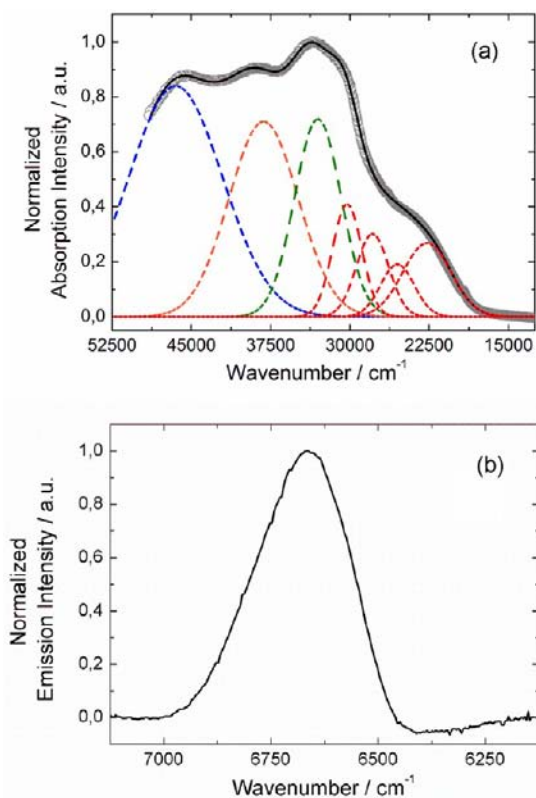

Figure 10. Experimental solid-state absorption and emission for **3** at room temperature. (a) UV−visible absorption spectrum (open circles), respective Gaussian deconvolutions (dashed lines) and best fit (full black line) $R = 0.9999$. (b) Emission spectrum in the NIR for $\lambda_{ex} = 20835$ cm^{-1} (480 nm).
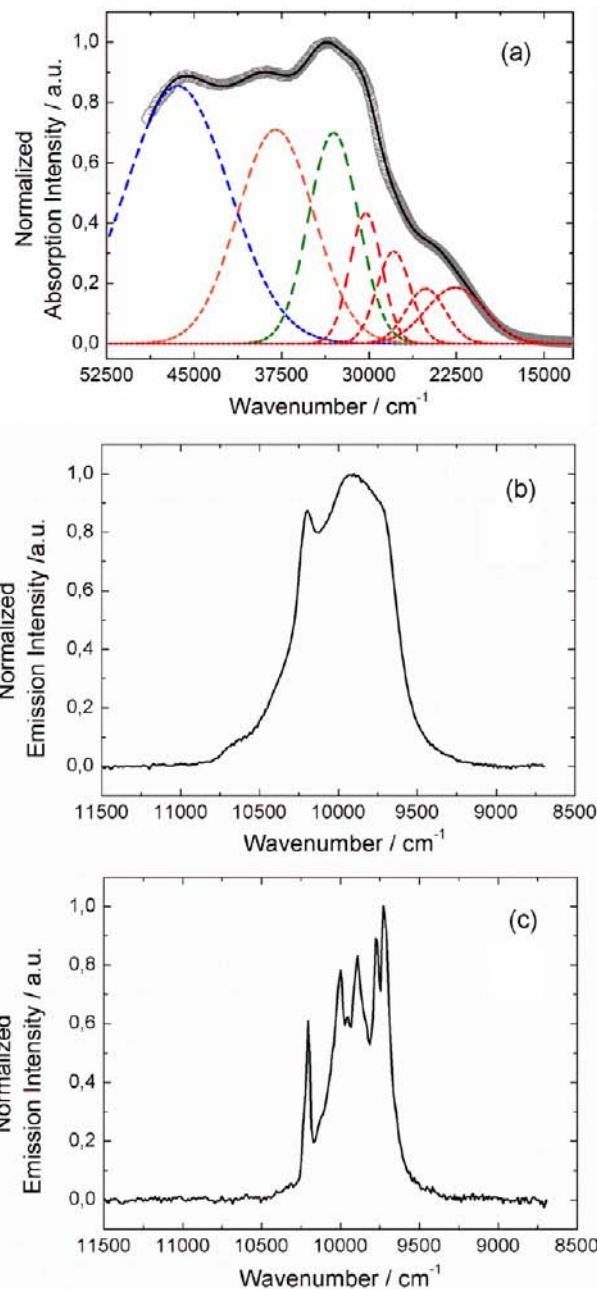

Figure 11. Experimental solid-state absorption and emission for **4**. (a) UV−visible absorption spectrum (open circles), respective Gaussian deconvolutions (dashed lines), and best fit (full black line) $R = 0.9997$. (b) Emission spectrum in the NIR for $\lambda_{ex} = 20835$ cm^{-1} (480 nm) at room temperature. (c) Emission spectrum in the NIR for $\lambda_{ex} = 20835$ cm^{-1} (480 nm) at 77 K.

This absorption band corresponds to $\pi-\pi^*$ intrahfac$^-$ excitations.[9c−e,11b] The complexations induce a weak red shift of the ligand-centered ILCT transitions due to the Lewis acid behavior of the Ln(hfac)$_3$ moieties enforcing the electron withdrawing character of the 2-pyridine-*N*-oxide fragments even if the electronic communication through the methylthio arms is expected to be very weak. Thus, the absorption bands are red-shifted to 700 cm^{-1} in the coordination complexes compared to those in **L**.

Emission Properties. One can note that the emission of the Tb^{III} and Dy^{III} can not be studied since the coordination complexes absorb strongly at the same energy (visible range)
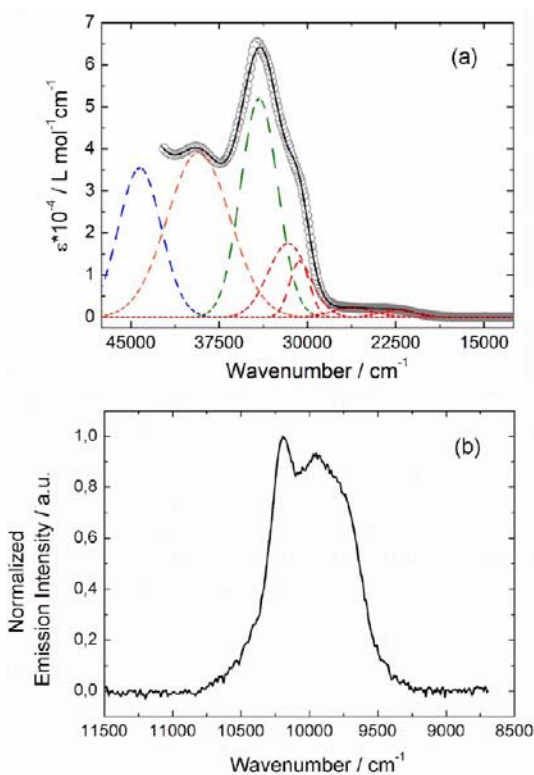
Figure 12. Experimental CHCl$_3$ solution absorption and emission for **4** at room temperature. (a) UV–visible absorption spectrum (open circles), respective Gaussian deconvolutions (dashed lines), and best fit (full black line) $R = 0.9997$. (b) Emission spectrum in the NIR for $\lambda_{\text{ex}} = 24390$ cm^{-1} (410 nm).

Table 5. Absorption Data for Coordination Complexes 3 and 4

experimental energies (cm^{-1})		
3 in solid state	**4 in solid state**	**4 in CHCl$_3$ solution**
22700	22600	22400
25500	25100	26200
27900	27900	30700
30300	30300	31700
33000	33000	34100
38200	38000	39200
46500	46400	44200

than the luminescence of such ions. Emission properties of **3** were measured in solid state at room temperature (Figure 10b). Upon irradiation at 20835 cm^{-1} in the lowest-energy absorption band, an emission centered at 6660 cm^{-1} (1502 nm) characteristic of the Er^{III} ^{4}I$_{13/2}$ → ^{4}I$_{15/2}$ transition is observed. No emission centered on the ligand is observed at lower energy, a sign that an efficient energy transfer occurs between the donor excited state and the luminescent state of the Er^{III} ion.

The compound **4** has been selected to study the Yb^{III} emission for simplicity because only one crystallographically independent molecule has been identified in the X-ray structure. Emission properties of **4** were first measured in solid state at room temperature (Figure 11b) and 77 K (Figure 11c), then in CHCl$_3$ solution (Figure 12b). At 77 K, the excitation of the sample with an energy of 20835 cm^{-1} leads to the Yb^{III} centered

luminescence. The signal is characterized by several peaks in the range 10500–9250 cm^{-1} (Figure 11c), which are assigned to the ^{2}F$_{5/2}$ → ^{2}F$_{7/2}$ excitation. At least, six transitions are clearly identified at the energies of 9728 cm^{-1}, 9775 cm^{-1}, 9891 cm^{-1}, 9950 cm^{-1}, 10000 cm^{-1}, and 10204 cm^{-1}. Keeping in mind that the maximum degeneracy of the ^{2}F$_{7/2}$ ground state is four (Kramer's doublets)[30] and that at low temperature only the M_J splitting of the ground state is observed, the six transitions experimentally observed could be explained by the presence of two crystallographically independent Yb^{III} ions with small changes in the coordination polyhedra even if the ideal symmetry remains C_{2v}. In fact the M_J state energies are correlated to the crystal field and symmetry around the lanthanide[31] and so each Yb1 and Yb2 has its own energy splitting of the M_J states. In this case, the maximum number of observed transitions could be equal to eight.

The M_J state splitting of the multiplet ground state ^{2}F$_{7/2}$ can also be probed with the molar magnetic susceptibility, χ_M, measurements. Indeed, the temperature dependence of χ_M varies with the thermal population of the crystal field levels. In the equivalent operators model the crystal field splitting is described by polynomials of the total angular momentum (J^2, J_z, J_+ and J_-):

$$
\begin{aligned}
\hat{H}_{\text{ZFS}} =\ & B_2^0\,\widehat{O_2^0} + B_2^2\,\widehat{O_2^2} \\
& + B_4^0\,\widehat{O_4^0} + B_4^2\,\widehat{O_4^2} + B_4^4\,\widehat{O_4^4} \\
& + B_6^0\,\widehat{O_6^0} + B_6^2\,\widehat{O_6^2} + B_6^4\,\widehat{O_6^4} + B_6^6\,\widehat{O_6^6}
\end{aligned}
$$

where the O_k^q's are the operator equivalents and the B_k^q's are connected to the crystal field parameters.[32] The perturbation due to the application of an external magnetic field can be easily estimated with the help of microcomputers and the magnetization calculated. In a C_{2v} environment all the B_k^q are nonzero,[33] but it would be unrealistic to fit the temperature dependence of $\chi_M T$ for **4** with all these 9 free parameters; especially for Yb^{III} derivatives with the ground state being only 8-fold degenerated. Then, to not overparametrize the procedure we have decided to fit the data with only axial parameters, that is, for $q = 0$. The drawback is that M_J remains a good quantum number, and no mixing occurs as it should in C_{2v} symmetry. The best fit (Figure 7) is obtained with $B_2^0 = 3.0003$ cm^{-1}, $B_4^0 = 0.5194$ cm^{-1}, and $B_6^0 = -3.473 \times 10^{-3}$ cm^{-1} with g$_J$ = 8/7 (fixed). The agreement is satisfactory with $R = 1/Npts\left((\chi_M T_{\text{exp}} - \chi_M T_{\text{calc}})^2 / \chi_M T_{\text{exp}}^2\right)^{1/2} = 4.84 \times 10^{-5}$ and with this set of parameters the field dependence of the magnetization at 2 K can be well reproduced (Supporting Information, Figure S4). The analysis of the energy levels reveal that the ground state corresponds to $M_J = \pm 5/2$, the first excited state to $M_J = \pm 3/2$ (+214 cm^{-1}), the second to $M_J = \pm 1/2$ (+632 cm^{-1}), and the last to $M_J = \pm 7/2$ (+651 cm^{-1}). This energy levels diagram must be compared to the splitting of the ^{2}F$_{5/2}$ → ^{2}F$_{7/2}$ excitation. The total splitting is largely overestimated by our fitting procedure (651 cm^{-1} against 478 cm^{-1} experimentally), but the energy gap between the ground and the first excited state (214 cm^{-1}) reproduces the energy separation between the two most energetic emission lines (204 cm^{-1}). These two lines at least provide a picture of the ground state splitting in these eight coordinated coordination polyhedra. The deficiency of the model at higher energies may come from the fact that (i) the model is developed for more symmetrical environment, D_{4d} instead of C_{2v}, and (ii) there are two Yb^{III} sites. Nevertheless, emission spectroscopy and magnetization measurements

provide same energy gap between the two low lying states of the $^2F_{7/2}$ ground state multiplet.[31b,c]

The luminescence spectrum of **4** at room temperature is broader than the one at 77 K, but the energies of the transitions remain the same. Nevertheless, the spectrum displays additional emission bands at higher energy (around 10373 cm^{-1} and 10627 cm^{-1}, Figure 11b) attributed to emission from a thermally populated higher crystal-field sublevel of the $^2F_{5/2}$ excited state (+179 cm^{-1} and +433 cm^{-1}).[34] The Yb^{III} centered luminescence for **4** is also observed in CHCl$_3$ solution upon irradiation at 24390 cm^{-1} (410 nm) (Figure 12b) in the maximum of the lowest-energy absorption band (Figure 12a). A comparison between the two emission spectra of **4** at room temperature (Figure 11b and 12b) shows that no shift of the emission components is observed. Both the presence of the luminescence of the Yb^{III} and the absence of a shift of the emission signal demonstrate the stability of **4** in CHCl$_3$ solution. Once again, no fluorescence of the ligand is observed in solid state and solution at room temperature and 77 K in the case of **4**.

CONCLUSIONS

Four tetranuclear coordination complexes of formula [Ln$_4$(hfac)$_{12}$(**L**)$_2$]$_n$·xCHCl$_3$·yC$_6$H$_{14}$ have been synthesized. Their crystalline structures reveal that the number of solvent molecules and the crystal packing (formation of dimers or 1D of **L**) depend on the nature of the lanthanide (size of the ionic radii). These compounds are the pure lanthanide polynuclear compounds involving TTF-based ligands with the highest nuclearity which have been reported until now.

Since the lanthanide centers are isolated in a magnetic point of view, all the tetranuclear compounds display classical paramagnetic behavior with significant crystal field effects.

The UV−visible absorption properties of **L** have been determined in CHCl$_3$ solution and rationalized by TD-DFT calculations. All the lowest energy absorption bands have been attributed to ILCT bands while the higher energy bands have been respectively attributed to ID and IA transitions.

Upon irradiation in the range 24390−20835 cm^{-1}, both compounds **3** and **4** display a metal-centered luminescence respectively attributed to $^4I_{13/2} \rightarrow {}^4I_{15/2}$ (6660 cm^{-1}) and $^2F_{5/2} \rightarrow {}^2F_{7/2}$ (signal centered around the value of 9966 cm^{-1}) excitations. In **4**, the emission spectrum at 77 K shows more than four transitions which could be attributed to the existence of two Yb1 and Yb2 ions with slightly different coordination polyhedra. Comparison of emission spectra at 77 K and room temperature show emission from a thermally populated higher crystal field sublevel of $^2F_{5/2}$. The change of redox states of the ligand in the complexes is in progress in our laboratory specially to probe the efficiency of the antenna of such ligand in the oxidized state and to reach the electronic conductivity property.

ASSOCIATED CONTENT

Ⓢ Supporting Information

Crystallographic information in CIF format, additional crystal data (Table S1−S3), simplified ORTEP view (Figure S1) and crystal packing (Figure S2) of **4b**, cyclic voltammetry for **1**−**4b** (Figure S3). First magnetization for **1**−**4** (Figure S4). Absorption spectra of **1** and **2** in solid state (Figure S5). This material is available free of charge via the Internet at http://pubs.acs.org.

AUTHOR INFORMATION

Corresponding Author

*E-mail: fabrice.pointillart@univ-rennes1.fr.

Notes

The authors declare no competing financial interest.

REFERENCES

(1) (a) Kobayashi, H.; Tomita, H.; Naito, T.; Kobayashi, A.; Sakai, F.; Watanabe, T.; Cassoux, P. *J. Am. Chem. Soc.* **1996**, *118*, 368. (b) Kobayashi, H.; Kobayashi, A.; Cassoux, P. *Chem. Soc. Rev.* **2000**, *29*, 325. (c) Kobayashi, A.; Fijiwara, E.; Kobayashi, H. *Chem. Rev.* **2004**, *104*, 5243 , and references therein. (d) Enoki, T.; Miyasaki, A. *Chem. Rev.* **2004**, *104*, 5449. (e) Kurmoo, M.; Graham, A. W.; Day, P.; Coles, S. J.; Hurtsthouse, M. B.; Caufield, J. M.; Singleton, J.; Ducasse, L.; Guionneau, P. *J. Am. Chem. Soc.* **1995**, *117*, 12209. (f) Coronado, E.; Day, P. *Chem. Rev.* **2004**, *104*, 5419 , and the references therein. (g) Ouahab, L.; Enoki, T. *Eur. J. Inorg. Chem.* **2004**, 933. (h) Lorcy, D.; Bellec, N.; Fourmigué, M.; Avavari, N. *Coord. Chem. Rev.* **2009**, *253*, 1398 , and references therein. (i) Fourmigué, M.; Ouahab, L. *Conducting and Magnetic Organometallic Molecular Materials*; Springer: Dordrecht, The Netherlands, 2009.

(2) (a) Graham, A. W.; Day, P. *J. Chem. Soc., Chem. Commun.* **1995**, 2061. (b) Kobayashi, H.; Kobayashi, A.; Cassoux, P. *Chem. Soc. Rev.* **2000**, *29*, 325. (c) Coronado, E.; Galan-Mascaros, J. R.; Gomez-Garcia, C. J.; Laukhin, V. *Nature* **2000**, *408*, 447. (d) Balicas, L.; Brooks, J. S.; Storr, K.; Uji, S.; Tokumoto, M.; Tanaka, H.; Kobayashi, H.; Kobayashi, A.; Barzykin, V.; Gor'kov, L. P. *Phys. Rev. Lett.* **2001**, 87.

(3) Carlin, R. L. *Magnetochemistry*; Springer: Berlin, Germany, 1986.

(4) (a) Sorace, L.; Benelli, C.; Gatteschi, D. *Chem. Soc. Rev.* **2011**, *40*, 3092. (b) Coulon, C.; Miyasaka, H.; Clerac, R. In *Single-Molecule Magnets and Related Phenomena*; Winpenny, R., Ed.; Springer-Verlag: Berlin, Germany, 2006; Vol. *122*, pp 163. (c) Sessoli, R.; Powell, A. K. *Coord. Chem. Rev.* **2009**, *253*, 2328. (d) Rinehart, J. D.; Fang, M.; Evans, W. J.; Long, J. R. *Nat. Chem.* **2011**, *3*, 538.

(5) (a) Sabbatini, N.; Guardigli, M.; Manet, I. *Handbook of the Physics and Chemistry of Rare Earths*; Elsevier: Amsterdam, The Netherlands, 1996; Vol. *23*, p 69. (b) Comby, S.; Bünzli, J.-C. G. *Handbook on the Physics and Chemistry of Rare Earths*; Elsevier BV: Amsterdam, The Netherland, 2007; Chapter 235, Vol. *37*. (c) Eliseeva, S. V.; Bünzli, J.-C. G. *Chem. Soc. Rev.* **2010**, *39*, 189. (d) Bünzli, J.-C. G.; Eliseeva, S. V. *J. Rare Earth* **2010**, *28*, 824.

(6) (a) Faulkner, S.; Pope, S. J. A.; Burton-Pye, B. P. *Appl. Spectrosc. Rev.* **2005**, *40*, 1. (b) Gunnlaugsson, T.; Stomeo, F. *Org. Biomol. Chem.* **2007**, *5*, 1999. (c) D'Aléo, A.; Bourdolle, A.; Bulstein, S.; Fauquier, T.; Grichine, A.; Duperray, A.; Baldeck, P. L.; Andraud, C.; Brasselet, S.; Maury, O. *Angew. Chem., Int. Ed.* **2012**, *51*, 6622.

(7) (a) Polman, A.; van Veggel, F. C. J. M. *J. Opt. Soc. Am. B* **2004**, *21*, 871. (b) Banerjee, S.; Huebner, L.; Romanelli, M. D.; Kumar, G. A.; Riman, R. E.; Emge, T. J.; Brennan, J. G. *J. Am. Chem. Soc.* **2005**, *127*, 15900. (c) Riman, R. E.; Kumar, G. A.; Banerjee, S.; Brennan, J. G. *J. Am. Ceram. Soc.* **2006**, *89*, 1809. (d) Kumar, G. A.; Riman, R. E.; Diaz Torres, L. A.; Banerjee, S.; Romanelli, M. D.; Emge, T. J.; Brennan, J. G. *Chem. Mater.* **2007**, *19*, 2937. (e) Banerjee, S.; Kumar, G. A.; Riman, R. E.; Emge, T. J.; Brennan, J. G. *J. Am. Chem. Soc.* **2007**, *129*, 5926. (f) Romanelli, M.; Kumar, G. A.; Emge, T. J.; Riman, R. E.; Brennan, J. G. *Angew. Chem., Int. Ed.* **2008**, *47*, 6049. (g) Song, L.; Liu, X.; Zhen, Z.; Chen, C.; Zhang, D. *J. Mater. Chem.* **2007**, *17*, 4586.

(8) (a) Imakubo, T.; Sawa, H.; Tajima, H.; Kato, R. *Synth. Met.* **1997**, *86*, 2047. (b) Tamura, M.; Matsuzaki, F.; Nishio, Y.; Kajita, K.; Kitazawa, T.; Mori, H.; Tanaka, S. *Synth. Met.* **1999**, *102*, 1716. (c) Dyachenko, O. A.; Kazheva, O. N.; Gritsenko, V. V.; Kushch, N. D. *Synth. Met.* **2001**, *120*, 1017. (d) Otsuka, T.; Cui, H.; Kobayashi, A.; Misaki, Y.; Kobayashi, H. *J. Solid State Chem.* **2002**, *168*, 444. (e) Kushch, N. D.; Kazheva, O.

N.; Gritsenko, V. V.; Buravov, L. I.; Van, K. V.; Dyachenko, O. A. *Synth. Met.* **2001**, *123*, 171. (f) Tamura, M.; Yamanaka, K.; Mori, Y.; Nishio, Y.; Kajita, K.; Mori, H.; Tanaka, S.; Yamaura, J. I.; Imakubo, T.; Kato, R.; Misaki, Y.; Tanaka, K. *Synth. Met.* **2001**, *120*, 1041. (g) Pointillart, F.; Maury, O.; Le Gal, Y.; Golhen, S.; Cador, O.; Ouahab, L. *Inorg. Chem.* **2009**, *48*, 7421.

(9) (a) Faulkner, S.; Burton-Pye, B. P.; Khan, T.; Martin, L. R.; Wray, S. D.; Skabara, P. J. *Chem. Commun.* **2002**, *16*, 1668. (b) Pope, S. J. A.; Burton-Pye, B. P.; Berridge, R.; Khan, T.; Skabara, P.; Faulkner, S. *Dalton Trans.* **2006**, 2907. (c) Pointillart, F.; Cauchy, T.; Maury, O.; Le Gal, Y.; Golhen, S.; Cador, O.; Ouahab, L. *Chem.—Eur. J.* **2010**, *16*, 11926. (d) Pointillart, F.; Bourdolle, A.; Cauchy, T.; Maury, O.; Le Gal, Y.; Golhen, S.; Cador, O.; Ouahab, L. *Inorg. Chem.* **2012**, *51*, 978. (e) D'Aléo, A.; Pointillart, F.; Ouahab, L.; Andraud, C.; Maury, O. *Coord. Chem. Rev.* **2012**, *256*, 1604.

(10) (a) Pointillart, F.; Le Gal, Y.; Golhen, S.; Cador, O.; Ouahab, L. *Chem.—Eur. J.* **2011**, *17*, 10397. (b) Pointillart, F.; Klementieva, S.; Kuropatov, V.; Le Gal, Y.; Golhen, S.; Cador, O.; Cherkasov, V.; Ouahab, L. *Chem. Commun.* **2012**, *48*, 714.

(11) (a) Cosquer, G.; Pointillart, F.; Le Gal, Y.; Golhen, S.; Cador, O.; Ouahab, L. *Chem.—Eur. J.* **2011**, *17*, 12502. (b) Cosquer, G.; Pointillart, F.; Le Guennic, B.; Le Gal, Y.; Golhen, S.; Cador, O.; Ouahab, L. *Inorg. Chem.* **2012**, *51*, 8488.

(12) (a) Liu, S.-X.; Dolder, S.; Pilkington, M.; Decurtins, S. *J. Org. Chem.* **2002**, *67*, 3160. (b) Jia, C.; Zhang, D.; Xu, Y.; Xu, X.; Hu, H.; Zhu, D. *Synth. Met.* **2003**, *132*, 249.

(13) Dolder, S.; Liu, S.-X.; Beurer, E.; Ouahab, L.; Decurtins, S. *Polyhedron* **2006**, *25*, 1514.

(14) Binet, L.; Fabre, J.-M.; Montginoul, C.; Simonsen, K. B.; Becher, J. *J. Chem. Soc., Perkin Trans.* **1996**, *1*, 783.

(15) Dias, S. I. G; Neves, A. I. S.; Rabaça, S.; Santos, I. C.; Almeida, M. *Eur. J. Inorg. Chem.* **2008**, 4728.

(16) (a) Liu, G.; Xue, G.; Yu, W.; Xu, W.; Fang, Q. *Acta Crystallogr., Sect. E* **2002**, *58*, o842. (b) Tanaka, M.; Shirasawa, K.; Taka, J.; Kashino, S. *Synth. Met.* **1999**, *103*, 2232. (c) Olivier, J.; Golhen, S.; Cador, O.; Ouahab, L. *C. R. Chim.* **2008**, *11*, 673. (d) Reinheimer, E. W.; Zhao, H.; Dunbar, K. R. *Synth. Met.* **2008**, *158*, 447. (e) Ding, Y.; Chen, Q.; Zhong, J.-C.; Munakata, M.; Konaka, H.; Ning, G.-L.; Wang, H.-Z. *Polyhedron* **2008**, *27*, 1393. (f) Olivier, J.; Golhen, S.; Swietlik, R.; Cador, C.; Pointillart, F.; Ouahab, L. *Eur. J. Inorg. Chem.* **2009**, 3282.

(17) Richarsdson, M. F.; Wagner, W. F.; Sands, D. E. *J. Inorg. Nucl. Chem.* **1968**, *30*, 1275.

(18) (a) Sheldrick, G. M. *SHELX97 - Programs for Crystal Structure Analysis*, Release 97-2; Institüt für Anorganische Chemie, University of Göttingen : Göttingen, Germany, 1998. (b) *SIR97*; Altomare, A.; Burla, M. C.; Camalli, M.; Cascarano, G. L.; Giacovazzo, C.; Guagliardi, A.; Moliterni, A. G. G.; Polidori, G.; Spagna, R. *J. Appl. Crystallogr.* **1999**, *32*, 115.

(19) Frisch, M. J.; Trucks, G. W.; Schlegel, H. B.; Scuseria, G. E.; Robb, M. A.; Cheeseman, J. R.; Scalmani, G.; Barone, V.; Mennucci, B.; Petersson, G. A.; Nakatsuji, H.; Caricato, M.; Li, X.; Hratchian, H. P.; Izmaylov, A. F.; Bloino, J.; Zheng, G.; Sonnenberg, J. L.; Hada, M.; Ehara, M.; Toyota, K.; Fukuda, R.; Hasegawa, J.; Ishida, M.; Nakajima, T.; Honda, Y.; Kitao, O.; Nakai, H.; Vreven, T.; Montgomery, Jr. J. A.; Peralta, J. E.; Ogliaro, F.; Bearpark, M.; Heyd, J. J.; Brothers, E.; Kudin, K. N.; Staroverov, V. N.; Kobayashi, R.; Normand, J.; Raghavachari, K.; Rendell, A.; Burant, J. C.; Iyengar, S. S.; Tomasi, J.; Cossi, M.; Rega, N.; Millam, J. M.; Klene, M.; Knox, J. E.; Cross, J. B.; Bakken, V.; Adamo, C.; Jaramillo, J.; Gomperts, R.; Stratmann, R. E.; Yazyev, O.; Austin, A. J.; Cammi, R; Pomelli, C.; Ochterski, J. W.; Martin, R. L.; Morokuma, K.; Zakrzewski, V. G.; Voth, G. A.; Salvador, P.; Dannenberg, J. J.; Dapprich, S.; Daniels, A. D.; Farkas, O.; Foresman, J. B.; Ortiz, J. V.; Cioslowski, J.; Fox, D. J. *Gaussian 09*, Revision A.02; Gaussian Inc.: Wallingford, CT, 2009.

(20) (a) Perdew, J. P.; Burke, K.; Ernzerhof, M. *Phys. Rev. Lett.* **1996**, *77*, 3865. (b) Adamo, C.; Barone, V. *J. Chem. Phys.* **1999**, *110*, 6158.

(21) Weigend, F.; Ahlrichs, R. *Phys. Chem. Chem. Phys.* **2005**, *7*, 3297.

(22) Tomasi, J.; Mennucci, B.; Cammi, R. *Chem. Rev.* **2005**, *105*, 2999.

(23) (a) Cossi, M.; Barone, V. *J. Chem. Phys.* **2001**, *115*, 4708. (b) Improta, R.; Barone, V.; Scalmani, G.; Frisch, M. J. *J. Chem. Phys.* **2006**, *125*, 054103.

(24) Allouche, A.-R. *J. Comput. Chem.* **2011**, *32*, 174.

(25) Svenstrup, N.; Rasmussen, K. M.; Hansen, J. K.; Becher, J. *Synthesis* **1994**, 809.

(26) Polasek, M.; Sedinova, M.; Kotek, J.; Vander Elst, L.; Muller, N. R.; Hermann, P.; Lukes, I. *Inorg. Chem.* **2009**, *48*, 455.

(27) (a) Muetterties, E. L.; Guggenberger, L. J. *J. Am. Chem. Soc.* **1974**, *96*, 1748. (b) Drew, M. G. B. *Coord. Chem. Rev.* **1977**, *24*, 179.

(28) Liu, S.-X.; Dolder, S.; Rusanov, E. B.; Stoeckli-Evans, H.; Decurtins, S. *C. R. Chim.* **2003**, *6*, 657.

(29) Kahn, O. *Molecular Magnetism*; VCH: Weinhem, Germany, 1993.

(30) Eliseeva, S. V.; Bünzli, J.-C. G. In *Lanthanide spectroscopy, Materials, and Bio-applications*; Hännen, P., Härmä, H., Eds.; Springer Verlag: Berlin, Germany, 2010; Vol. 7, Chapter 1.

(31) (a) Rinehart, J. D.; Long, J. R. *Chem. Sci.* **2011**, *2*, 2078. (b) Cucinotta, G.; Perfetti, M.; Luzon, J.; Etienne, M.; Car, P. E.; Caneschi, A.; Calvez, G.; Bernot, K.; Sessoli, R. *Angew. Chem., Int. Ed.* **2012**, *51*, 1606. (c) Long, J.; Vallat, R.; Ferreira, R. A. S.; Carlos, L. D.; Almeida Paz, F. A.; Guari, Y.; Larionova, J. *Chem. Commun.* **2012**, *48*, 9974. (d) Liu, J.-L.; Yuan, K.; Leng, J.-D.; Ungur, L.; Wernsdorfer, W.; Guo, F.-S.; Chibotaru, L. F.; Tong, M.-L. *Inorg. Chem.* **2012**, *51*, 8538.

(32) (a) Orbach, R. *Proc. Phys. Soc. A* **1961**, *264*, 458. (b) Rudowicz, C. *J. Phys. C: Solid State Phys.* **1985**, *18*, 1415.

(33) Görlder-Walrand, C.; Binnemans, K. In *Handbook on the Physics and Chemistry of Rare Earths*; Elsevier North Holland: Amsterdam, The Netherlands, 1996; Vol. 23, p 121.

(34) Ziessel, R. F.; Ulrich, G.; Charbonnière, L.; Imbert, D.; Scopelliti, R.; Bünzli, J.-C. G. *Eur.—J. Chem.* **2006**, *12*, 5060.